Experiments in Fluids 35 (2003) 372–379
DOI 10.1007/s00348-003-0686-x

Comparison of three roughness function determination methods

M. P. Schultz, A. Myers

Abstract Three methods have been used to experimentally determine the roughness function (ΔU^+) for several rough surfaces. These include the rotating disk, the towed plate, and the velocity profile methods. The first two are indirect methods in as much as they rely on measurements of overall torque or resistance and boundary layer similarity laws to obtain ΔU^+, whereas the velocity profile method provides a direct measurement of ΔU^+. The present results indicate good agreement between the towed plate and the velocity profile methods for all of the surfaces tested. Tests for the rotating disk were carried out at much higher unit Reynolds numbers. Using this method, the results for sandpaper rough surfaces agree within their uncertainty with a Nikuradse-type roughness function in the fully rough regime, while a spray painted surface agrees with a Colebrook-type roughness function.

Nomenclature

B	smooth wall log-law intercept, =5.0
C_F	overall frictional resistance coefficient, $= (F_D)/\left(\frac{1}{2}\rho U_e^2 S\right)$
C_f	skin-friction coefficient, $= (\tau_o)/\left(\frac{1}{2}\rho U_e^2\right)$
C_m	torque coefficient, $=(2M)/(\rho R^5(\phi\omega)^2)$
F_D	drag force
k	arbitrary measure of roughness height
K	acceleration parameter, $= \frac{\nu}{U_e^2}\frac{dU_e}{dx}$
L	plate length
M	torque
N	number of samples or replicates
R	disk radius
R_a	centerline average roughness height, $= \frac{1}{N}\sum_{i=1}^{N}\lvert y_i\rvert$
R_q	root mean square roughness height, $= \sqrt{\frac{1}{N}\sum_{i=1}^{N} y_i^2}$
R_t	maximum peak to through height, $=y_{max}-y_{min}$
R_z	ten point roughness height, $= \sum_{i=1}^{5}(y_{max\,i} - y_{min\,i})$
Re_L	Reynolds number based on plate length, $=U_eL/\nu$
Re_R	Reynolds number based on disk radius, $=\phi\omega R^2/\nu$
Re_θ	momentum thickness Reynolds number, $=U_e\theta/\nu$
S	wetted surface area
U	mean velocity in the x direction
U_e	freestream velocity relative to surface
U_τ	friction velocity, $= \sqrt{\tau_o/\rho}$
u'	streamwise fluctuating velocity
v'	wall-normal fluctuating velocity
x	streamwise distance from plate leading edge
y	normal distance from the boundary
δ	boundary layer thickness
ΔU^+	roughness function
$\Delta U^{+\prime}$	roughness function slope, $=d(\Delta U^+)/d(\ln k^+)$
ε	wall datum offset
ϕ	swirl factor, $\left(\frac{1}{\sqrt{C_m}}\right)_\infty \Big/ \left(\frac{1}{\sqrt{C_m}}\right)_{en}$
κ	von Kármán constant, =0.41
ν	kinematic viscosity of the fluid
Π	wake parameter
θ	momentum thickness, $= \int_0^\delta \left(1-\frac{U}{U_e}\right)^2 dy$
ρ	density of the fluid
τ_o	wall shear stress
ω	angular velocity

Superscript

+	inner variable (normalized with U_τ or U_τ/ν)

Subscripts

en	disk rotating in enclosed tank
min	minimum value
max	maximum value
R	rough surface
S	smooth surface
∞	disk rotating in unconfined fluid

Received: 19 December 2002 / Accepted: 25 June 2003
Published online: 23 August 2003

M. P. Schultz (✉), A. Myers
Department of Naval Architecture and Ocean Engineering,
United States Naval Academy, Annapolis, MD21402, USA
E-mail: mschultz@usna.edu

MPS would like to thank the Office of Naval Research for financial support of this research under the direction of Dr. Steve McElvaney. The authors would also like to acknowledge the ongoing financial support of the disk drag measurements from Mr. William Stoffel (NSWC-Carderock, Code 981, Shipboard R&D Office) and Dr. Alan Roberts (CNO, N420, Energy Plans & Policy). Thanks, as well, to Dr. Eric Holm, Ms. Elizabeth Haslbeck, and Ms. Jean Montemarano from NSWC-Carderock (Code 641) for allowing us to use the rotating disk facility and for providing technical guidance. Many thanks go to Mr. Steve Enzinger, Mr. Don Bunker, and the USNA Hydromechanics Laboratory and Technical Support Division staff for assisting with the project. We are also indebted to Prof. Michelle Koul for helping with the laser profilometry.

Report Documentation Page

Form Approved
OMB No. 0704-0188

1. REPORT DATE	2. REPORT TYPE	3. DATES COVERED
DEC 2002		**00-00-2002 to 00-00-2002**

4. TITLE AND SUBTITLE	5a. CONTRACT NUMBER
Comparison of three roughness function determination methods	5b. GRANT NUMBER
	5c. PROGRAM ELEMENT NUMBER
6. AUTHOR(S)	5d. PROJECT NUMBER
	5e. TASK NUMBER
	5f. WORK UNIT NUMBER
7. PERFORMING ORGANIZATION NAME(S) AND ADDRESS(ES) **United States Naval Academy,Department of Naval Architecture and Ocean Engineering,Annapolis,MD,21402**	8. PERFORMING ORGANIZATION REPORT NUMBER
9. SPONSORING/MONITORING AGENCY NAME(S) AND ADDRESS(ES)	10. SPONSOR/MONITOR'S ACRONYM(S)
	11. SPONSOR/MONITOR'S REPORT NUMBER(S)

12. DISTRIBUTION/AVAILABILITY STATEMENT
Approved for public release; distribution unlimited

13. SUPPLEMENTARY NOTES

14. ABSTRACT

Three methods have been used to experimentally determine the roughness function (DU+) for several rough surfaces. These include the rotating disk, the towed plate, and the velocity profile methods. The first two are indirect methods in as much as they rely on measurements of overall torque or resistance and boundary layer similarity laws to obtain DU+, whereas the velocity profile method provides a direct measurement of DU+. The present results indicate good agreement between the towed plate and the velocity profile methods for all of the surfaces tested. Tests for the rotating disk were carried out at much higher unit Reynolds numbers. Using this method, the results for sandpaper rough surfaces agree within their uncertainty with a Nikuradse-type roughness function in the fully rough regime, while a spray painted surface agrees with a Colebrook-type roughness function.

15. SUBJECT TERMS

16. SECURITY CLASSIFICATION OF:			17. LIMITATION OF ABSTRACT	18. NUMBER OF PAGES	19a. NAME OF RESPONSIBLE PERSON
a. REPORT	b. ABSTRACT	c. THIS PAGE			
unclassified	**unclassified**	**unclassified**	**Same as Report (SAR)**	**8**	

1 Introduction

Wall-bounded turbulent flows over roughness occur in a multitude of situations in both the natural environment and in engineering applications. Examples range from wind over plant canopies to boundary layers on ships and aircraft. Since surface roughness affects not only the near wall mean velocity profile but also the resulting drag and heat transfer, it has been the subject of a great deal of research (e.g., Nikuradse 1933; Clauser 1954; Hama 1954; Ligrani and Moffat 1986; Raupach et al. 1991; Antonia and Krogstad 2001).

The mean velocity profile in the inner region of the smooth wall turbulent boundary layer is given by the classical log-law.

$$U^+ = \frac{1}{\kappa}\ln(y^+) + B \tag{1}$$

Clauser (1954) demonstrated that the primary effect of surface roughness was to cause a downward shift in the log-law. This downward shift, ΔU^+, is called the roughness function. The generalized log-law for rough and smooth walls is therefore given as

$$U^+ = \frac{1}{\kappa}\ln(y+\varepsilon)^+ + B - \Delta U^+ \tag{2}$$

For so-called "k-type" roughness, ΔU^+ is a function of the roughness Reynolds number, k^+, defined as the ratio of the roughness length scale, k, to the viscous length scale, ν/U_τ. Once $\Delta U^+ = \Delta U^+(k^+)$ for a given rough surface is known, it can be used in a boundary layer code or a similarity law analysis to predict the drag of any body covered with that roughness (Granville 1958). However, determining the roughness function is not without difficulty. There are two primary reasons for this. First, the roughness function is not universal for all roughness types. Nikuradse's (1933) pipe flow experiments with closely packed, uniform sand indicate this roughness type has a universal roughness function with k simply being the diameter of the individual sand grains. However, the roughness functions for most naturally occurring surfaces do not behave like closely packed, uniform sand. Colebrook (1939) demonstrated this in a study of the irregular surface roughness in pipes resulting from the manufacturing process. The other primary difficulty is specifying a proper roughness length scale, k, for a given roughness geometry. Granville (1987) states that more than one roughness length scale may be required to adequately represent an arbitrarily rough surface. For these reasons, determining the roughness function for a generic surface requires experimental tests (Grigson 1992).

Various experimental methods have been offered for determining ΔU^+ for rough surfaces. The most evident is to directly measure ΔU^+ using the mean velocity profile in the log-law region over the roughness (Clauser 1954). However, the determination of U_τ for a rough wall profile is more prone to error due to the two additional parameters (the position of the y origin and ΔU^+) that must also be found when fitting the profile (Acharya et al. 1986). There are several indirect methods for finding ΔU^+ as well. These include measuring the pressure drop in fully developed pipe or channel flow (Nikuradse 1933), the torque on rotating disks (Granville 1982), and the drag on towed flat plates (Granville 1987). Using these measurements and boundary layer similarity laws, ΔU^+ can be determined. The goal of the present experimental investigation is to compare the roughness functions obtained using three of these methods; the velocity profile, rotating disk, and towed plate methods.

2 Experimental methods and conditions

In this study, four surfaces were tested for each of the roughness function determination methods. These included a baseline smooth surface, a 60-grit sandpaper surface, a 220-grit sandpaper surface, and a sprayed epoxy surface. The surface profiles of the rough surfaces were measured using a laser diode point range sensor (model No. PRS 40, CyberOptics Corp., Minneapolis, Minn., USA) laser profilometer system mounted to a Parker Daedal (model No. 106012BTEP-D3L2C4M1E1, Parker Hannifin Corp., Irwin, Penn., USA) two-axis traverse with a resolution of 5 μm. The resolution of the sensor is 1 μm with a laser spot diameter of 10 μm. Data were taken over a sampling length of 50 mm and were digitized at a sampling interval of 25 μm. Ten linear profiles were taken on each of the test surfaces. The sandpaper surfaces were constructed from the same sheet of sandpaper, so the roughness on these surfaces agreed within their uncertainty. The sprayed epoxy surface used in each method varied somewhat because of differences in paint application. The mean roughness statistics for each of the test surfaces along with their 95% precision confidence limits are given in Table 1.

2.1 Velocity profile method

The velocity profile method experiments were carried out in the closed circuit water tunnel facility at the United States Naval Academy Hydromechanics Laboratory. The test section is 40 cm by 40 cm in cross-section and is 1.8 m in length, with a tunnel velocity range of 0–6.0 m/s. In the present study, the freestream velocity was varied between ~1.0 m/s and 3.5 m/s (Re_x=1.4×10^6–4.9×10^6). Flow management devices include turning vanes placed in the tunnel corners and a honeycomb flow straightener in the settling chamber. The honeycomb has 19 mm cells that are 150 mm in length. The area ratio between the settling chamber and the test section is 20:1, and the resulting

Table 1. Roughness statistics

Specimen	R_a (μm)	R_q (μm)	R_t (μm)	R_z (μm)
Smooth	NA	NA	NA	NA
60-Grit sandpaper	126±5	160±7	983±89	921±82
220-Grit sandpaper	30±2	38±2	275±17	251±14
Epoxy—velocity profile	9±1	12±1	76±8	71±7
Epoxy—rotating disk	15±1	19±1	128±13	120±13
Epoxy—towed plate	10±1	17±1	135±7	130±6

Uncertainties represent the 95% confidence precision bounds

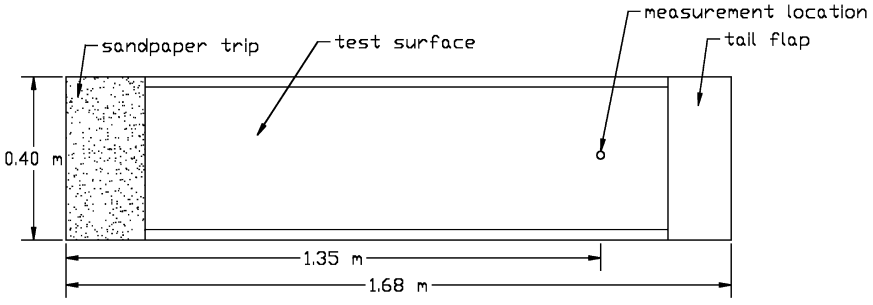

Fig. 1. Schematic of the flat plate test fixture for the velocity profile method

freestream turbulence intensity in the test section is ~0.5%.

The test specimens were inserted into a flat plate test fixture mounted horizontally in the tunnel. The test fixture, shown in Fig. 1, is similar to that used by Schultz and Flack (2003). The fixture is 0.40 m in width, 1.68 m in length, and 25 mm thick. It is constructed of a high density foam core covered with carbon fiber reinforced plastic skins and was mounted horizontally in the tunnel's test section along its centerline. The leading edge of the test fixture is elliptically shaped with an 8:1 ratio of the major and minor axes. The forward most 200 mm of the plate is covered with 36-grit sandpaper to trip the developing boundary layer. The use of a strip of roughness was shown by Klebanoff and Diehl (1951) to provide effective boundary layer thickening and a fairly rapid return to self-similarity. The test specimen mounts flush into the test fixture and its forward edge is located immediately downstream of the trip. The removable test specimens are fabricated from 12 mm thick cast acrylic sheet 350 mm in width and 1.32 m in length. The boundary layer profiles presented here were taken 1.35 m downstream of the leading edge of the test fixture. Profiles taken from 0.75 m to the measurement location confirmed that the flow had reached self-similarity. The trailing 150 mm of the flat plate fixture is a movable tail flap. This was set with the trailing edge up at ~5° in the present experiments to prevent separation at the leading edge of the plate. The physical growth of the boundary layer and the inclined tail flap created a slightly favorable pressure gradient at the measurement location. The acceleration parameter (K) varied from 7.4×10^{-8} at the lowest freestream velocity to 2.0×10^{-8} at the highest freestream velocity. The pressure gradient did not vary significantly between the test specimens.

Velocity measurements were made using a TSI IFA550 (TSI Inc., St. Paul, Minn., USA) two-component, fiber-optic LDV system. The LDV used a four-beam arrangement and was operated in backscatter mode. The probe volume diameter was ~90 μm, and its length was ~1.3 mm. The viscous length (ν/U_τ) varied from a minimum of 5 μm for 60-grit sandpaper at the highest Reynolds number to 24 μm for the smooth wall at the lowest Reynolds number. The diameter of the probe volume, therefore, ranged from 3.8 to 18 viscous lengths in the present study. The LDV probe was mounted on a three-axis traverse unit (Velmex Inc., Bloomfield, N.Y., USA). The traverse allowed the position of the probe to be maintained to ±10 μm in all directions. In order to facilitate two-component, near wall measurements, the probe was tilted downwards at an angle of 4° to the horizontal and was rotated 45° about its axis. The tilting of the LDV probe led to a small bias error in the v' measurements because of the introduction of the w' fluctuations in the measurement plane. The error in the measured Reynolds shear stress caused by tilting was <1%. Velocity measurements were conducted in coincidence mode with 20,000 random samples per location. Doppler bursts for the two channels were required to fall within a 50 μs coincidence window or the sample was rejected.

In this study, the friction velocity, U_τ, for the smooth surface was found using the Clauser chart method with log-law constants k=0.41 and B=5.0. For the rough walls, U_τ and ϵ were obtained using a procedure based on the modified Clauser chart method given by Perry and Li (1990). For the rough surfaces the top plane of the roughness elements was taken to be y=0. The wall datum shift, ϵ, is the distance below top plane of the roughness elements that U=0. In the present experiments, ϵ/R_t generally ranged between 0.25 and 0.35 for the roughness types tested. For all the test surfaces, the total stress method was also used to verify U_τ. This method assumes a constant stress region equal to the wall shear stress exists in the inner layer of the boundary layer. If the viscous and turbulent stress contributions are added together, an expression for U_τ may be calculated as the following evaluated at the total stress plateau in the inner layer:

$$U_\tau = \left[\nu\frac{\partial U}{\partial y} - \overline{u'v'}\right]^{1/2} \tag{3}$$

In all cases the agreement between the Clauser chart and total stress methods was well within their uncertainty. The roughness function for the rough surfaces was obtained as the difference between the log-law intercept for the smooth and the rough walls. The test conditions for the velocity profile method are given in Table 2.

2.2 Rotating disk method

The rotating disk experiments were conducted in the disk drag facility at the Naval Surface Warfare Center, Carderock Division. A schematic of the facility is shown in Fig. 2. The torque measurements were made on 22.9 cm diameter, 5 mm thick aluminum disks, coated with the specified roughness, rotated in the enclosed acrylic tank. The tank is 25 cm in height and 33 cm in diameter. The angular velocity of the disks was varied between 700 and

Table 2. Experimental test conditions for velocity profile method

Specimen	U_e (ms^{-1})	Re_θ	$C_f\times10^3$ Clauser	$C_f\times10^3$ Total stress	δ (mm)	δ^* (mm)	H	Π
Smooth	0.94	2,950	3.44	3.32	28	3.8	1.30	0.36
	2.60	7,020	2.99	3.04	26	3.2	1.27	0.30
	2.99	8,080	2.92	2.82	27	3.2	1.26	0.30
	3.58	9,680	2.82	2.77	26	3.2	1.26	0.30
60-Grit sandpaper	0.93	3,720	4.82	4.55	33	5.1	1.38	0.40
	2.53	10,600	5.04	5.29	33	5.5	1.42	0.38
	3.12	13,800	4.87	5.09	33	5.9	1.44	0.44
	3.58	16,400	4.84	5.13	34	6.1	1.43	0.45
220-Grit sandpaper	0.95	3,420	3.52	3.66	33	4.7	1.36	0.55
	2.60	8,930	3.79	3.90	29	4.3	1.34	0.38
	3.07	11,000	3.89	3.77	30	4.5	1.36	0.41
	3.63	12,900	3.85	3.69	30	4.6	1.36	0.44
Epoxy	0.93	3,170	3.40	3.31	31	4.1	1.30	0.42
	2.50	8,080	3.05	3.14	31	3.8	1.29	0.37
	3.11	10,500	2.94	2.98	31	4.0	1.29	0.45
	3.59	11,900	2.95	2.87	31	4.0	1.29	0.42

1,500 rpm (Re_R=9.0×10^5–2.0×10^6). This was measured using a Scientific Atlanta/Spectral Dynamics model 13134/13135 GPT stroboscopic tachometer (Spectral Dynamics, San Jose, Calif., USA). The combined precision and bias error of the device is <1% of the reading. A Baldor model 3445 DC motor (Baldor Electric Co., Fort Smith, Ariz., USA) rated at 1 hp powers the rotating disk facility. Feedback control to the Baldor model BD154 motor controller was used to hold the angular velocity constant based on input from the tachometer. The torque was measured by means of a Lebow model 1104-50 slip ring-type torque sensor (Lebow Products, Troy, Mich., USA). This sensor has a range of 0–5.7 N m with a combined bias uncertainty of ±0.05% of full scale. The working fluid in the experiments was fresh water, and the temperature was monitored to within ±0.05°C during the course of the experiments using a thermocouple logging to the A/D system. Data, which included temperature, angular velocity, and torque were gathered at a sampling rate of 1,000 Hz and were digitized using a 16-bit A/D converter.

Before data were collected on the surfaces of interest, the tare torque values caused by frictional resistance in the bearings and hydrodynamic torque on the shaft itself were measured. This was accomplished by rotating the shaft, without the disk, in the tank of water. This was done by setting the angular velocity to 700 rpm and holding it there for 120 s. Since some time was necessary for the tank conditions to reach an equilibrium state, only data from the final 30 s were used. This procedure was then repeated for 900, 1,100, 1,300, and 1,500 rpm. Replicate measurements at all of the angular velocities were made. The test disks were then attached to the shaft, and a similar process was repeated for the four test surfaces.

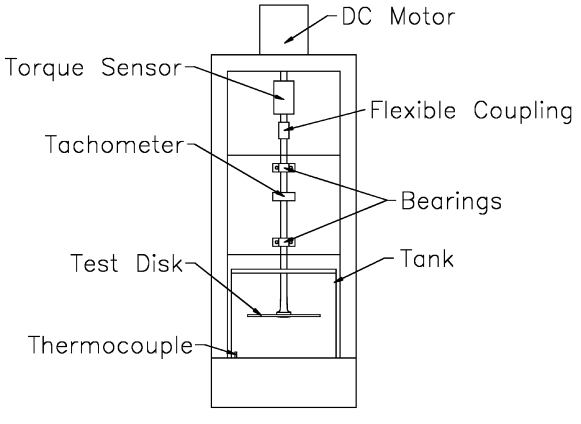

Fig. 2. Schematic of rotating disk test apparatus

It should be noted that spinning the disk in the confined tank sets up a mean tangential flow in the fluid. The result is that the actual angular velocity of the disk relative to the fluid is somewhat less than the angular velocity of the disk itself. Granville (1982) states that this can be corrected for by comparing C_m values measured for a given surface in the tank to those measured for the same surface in a very large body of water (i.e., unconstrained fluid) at the same value $Re_R(C_m)^{1/2}$. He terms this the swirl factor for the test facility, which is defined as follows:

$$\phi = \left(\frac{1}{\sqrt{C_m}}\right)_\infty \Big/ \left(\frac{1}{\sqrt{C_m}}\right)_{en} \tag{4}$$

The test facility used in this study was previously used by Loeb et al. (1984), who found ϕ=0.854 over a wide range of $Re_R(C_m)^{1/2}$. This value of ϕ was, therefore, used in the present study.

The roughness functions for the rotating disk data were calculated using the similarity law analysis of Granville (1982). This procedure involves comparing the C_m values of smooth and rough disks at the same value of $Re_R(C_m)^{1/2}$. The resulting equations for k^+ and ΔU^+ are given in Eqs. (5) and (6), respectively.

$$k^+ = \left(\frac{k}{R}\right)\sqrt{\frac{5}{8\pi}}Re_R\sqrt{C_m}\left\{1 - \left[\frac{2}{\kappa} - \Delta U^{+\prime}\right]\left(\sqrt{\frac{C_m}{40\pi}}\right)_R\right\} \tag{5}$$

$$\Delta U^+ = \sqrt{\frac{8\pi}{5}}\left[\left(\frac{1}{\sqrt{C_m}}\right)_S - \left(1\sqrt{C_m}\right)_R\right] + \frac{1}{5}\Delta U^{+\prime} \tag{6}$$

Details of the development of these equations are given in Granville (1982). It should be noted that the solutions to

both of the equations are iterative. Initially, $\Delta U^{+\prime}$ is taken to be zero and the equations are solved. Based on this solution, $\Delta U^{+\prime}$ is calculated and the procedure repeated until the solution converges.

2.3 Towed plate method

The towed plate experiments were conducted in the 115-m long towing tank facility at the United States Naval Academy Hydromechanics Laboratory using an experimental method similar to that used by Schultz (2002). The width and depth of the tank are 7.9 m and 4.9 m, respectively. The towing carriage has a velocity range of 0–7.6 m/s. In the present investigation, the towing velocity was varied between 2.0 m/s and 3.8 m/s (Re_L=2.8×10^6–5.5×10^6). The velocity of the towing carriage was measured and controlled using an encoder on the rails that produce 4,000 pulses/m. Using this system, the precision uncertainty in the mean velocity measurement was <0.02% over the entire velocity range tested. The working fluid in the experiments was fresh water, and the temperature was monitored to within ±0.05°C during the course of the experiments using a thermocouple with digital readout.

Figure 3 shows a schematic of the test fixture and plate. The flat test plate was fabricated from 304 stainless steel sheet stock and measured 1.52 m in length, 0.76 m in width, and 3.2 mm in thickness. Both the leading and trailing edges were filleted to a radius of 1.6 mm. No tripping device was used to stimulate transition. The overall drag of the plate was measured using a model HI-M-2, modular variable-reluctance displacement force transducer manufactured by Hydronautics Inc. An identical force transducer, rotated 90° to the drag gage, was included in the test rig to measure the side force on the plate. The purpose of the side force gage was to ensure precise alignment of the plate. This was accomplished by repeatedly towing the plate at a constant velocity and adjusting the yaw angle of the test fixture to minimize the side force. Once this was done, no further adjustments were made to the alignment over the course of the experiments. The side force was monitored throughout to confirm that the plate alignment did not vary between test surfaces. Both of the force transducers used in the experiments had load ranges of 0–89 N. The combined bias uncertainty of the gages is ±0.25% of full scale. Data were gathered at a sampling rate of 100 Hz and were digitized using a 16-bit A/D converter. The length of the towing tank dictated the sampling duration. This ranged from ~30 s of data per test run at the lowest Reynolds number to ~11 s of at the highest Reynolds number. The overall drag was first measured with 590 mm of the plate submerged. This was repeated with 25 mm of the plate submerged in order to find the wavemaking resistance tare. The difference between the two was taken to be the frictional resistance on the two 565 mm wide by 1.52 m long faces of the plate.

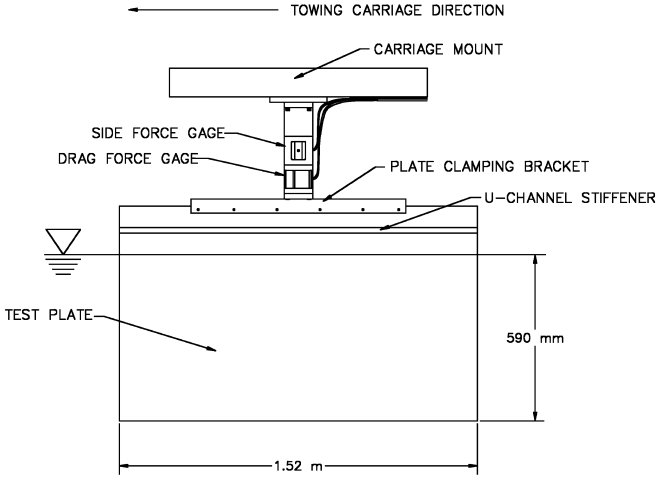

Fig. 3. Schematic of the flat plate test fixture for the towed plate method

The roughness functions for the towed plate data were calculated using the similarity law analysis of Granville (1987). This procedure involves comparing the C_F values of smooth and rough plates at the same value of $Re_L C_F$. The resulting equations for k^+ and ΔU^+ are given in Eqs. (7) and (8), respectively.

$$k^+ = \left(\frac{k}{L}\right)\left(\frac{Re_L C_F}{2}\right)\left(\sqrt{\frac{2}{C_F}}\right)_R \times \left[1 - \frac{1}{\kappa}\left(\sqrt{\frac{C_F}{2}}\right)_R + \frac{1}{\kappa}\left(\frac{3}{2\kappa} - \Delta U^{+\prime}\right)\left(\frac{C_F}{2}\right)_R\right] \quad (7)$$

$$\Delta U^+ = \left(\sqrt{\frac{2}{C_F}}\right)_S - \left(\sqrt{\frac{2}{C_F}}\right)_R - 19.7\left[\left(\sqrt{\frac{C_F}{2}}\right)_S - \left(\sqrt{\frac{C_F}{2}}\right)_R\right] - \frac{1}{\kappa}\Delta U^{+\prime}\left(\sqrt{C_{\frac{F}{2}}}\right)_R \quad (8)$$

Details of the development of these equations are given in Granville (1987). Again, the solutions to both of the equations are iterative. Initially, $\Delta U^{+\prime}$ is taken to be zero and the equations are solved. Based on this solution, $\Delta U^{+\prime}$ is calculated and the procedure repeated until the solution converges.

2.4 Uncertainty estimates

Precision uncertainty estimates for all of the measurements in this investigation were made through repeatability tests. This involved conducting repeated experiments for a given surface condition using each of the testing methods. In order to estimate the 95% precision confidence limits for a measured parameter, its standard deviation was multiplied by the two-tailed t value for (N−1) degrees of freedom, as given by Coleman and Steele (1995). These uncertainties were then combined with the estimated bias uncertainties using standard error propagation methods (Moffat 1988) to find the overall 95% confidence limits for the calculated parameters. The resulting overall 95% confidence limits for C_m and C_F were both ±2%. The resulting overall 95% confidence limits for C_f were ±4% for the smooth wall and ±7% for the rough walls using the Clauser chart method. The C_f results using the total stress method (Eq. 3) agreed within their uncertainty with those obtained using the Clauser chart method. The resulting uncertainties in ΔU^+ were ±10% or 0.2 (whichever was greater), ±9% or 0.3 (whichever was

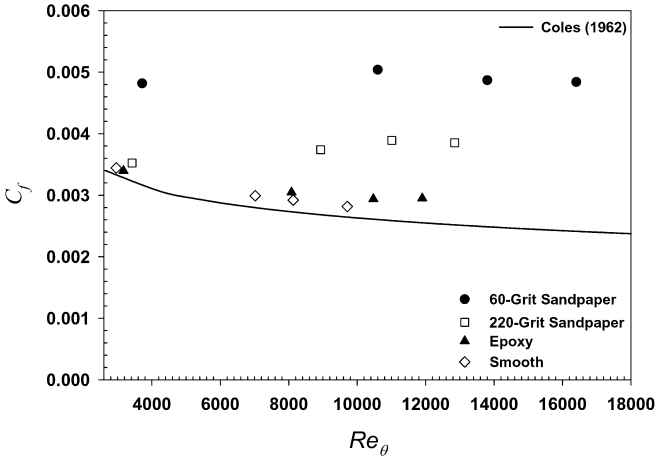

Fig. 4. Skin-friction coefficient vs. momentum thickness Reynolds number for the velocity profile method. (Overall uncertainty in C_f: smooth wall, ±4%; rough walls, ±7%)

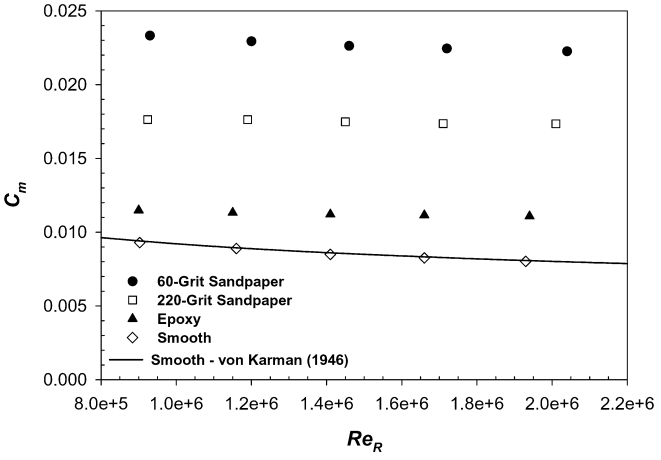

Fig. 6. Torque coefficient vs. Reynolds number for the rotating disk method. (Overall uncertainty in C_m: ±2%)

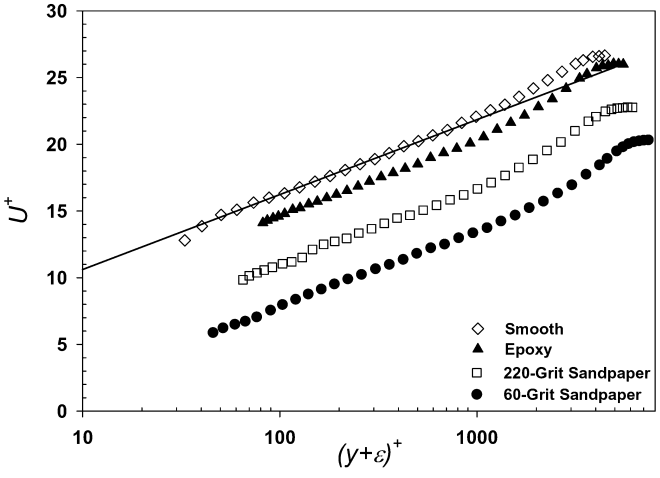

Fig. 5. Mean velocity profiles in wall coordinates for all surfaces at the highest Re_x. (Overall uncertainty in U^+: smooth wall, ±3%; rough wall, ±5%)

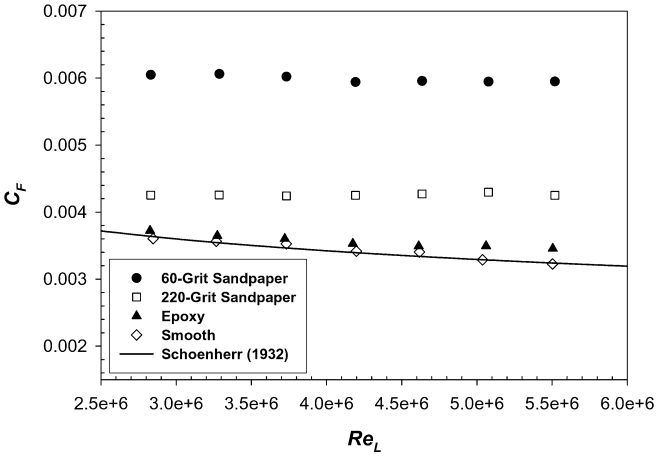

Fig. 7. Frictional resistance coefficient vs. Reynolds number for the towed plate method. (Overall uncertainty in C_F: ±2%)

greater), and ±12% or 0.2 (whichever was greater) for the velocity profile, rotating disk, and towed plate methods, respectively.

3 Results and discussion

The skin-friction results for the velocity profile method are shown in Fig. 4. The smooth wall results of Coles (1962) are presented for comparison. Both sandpaper rough surfaces exhibited a significant increase in C_f over the entire range of Re_θ. For example, at the highest Reynolds number, C_f was 86% higher for the 60-grit sandpaper and was 42% higher for the 220-grit sandpaper than the smooth wall values. The C_f values for epoxy surface are observed to rise only slightly above the smooth wall values as Re_θ increases. At the highest Reynolds number, the C_f for the epoxy surface is 8% higher than the smooth wall value, which is still within the combined uncertainty of the measurements.

Figure 5 shows the mean velocity profiles in wall variables for all of the test surfaces at the highest Re_x tested (~4.9×10^6). The results show that the smooth profile follows the classical log-law (Eq. 1) well in the overlap region. The three rough surfaces also display a linear log region that is shifted by ΔU^+ below the smooth profile (Eq. 2). A trend of increasing ΔU^+ with increasing roughness height is observed in the results.

Figure 6 shows the results of the rotating disk experiments. Shown for comparison is the empirical relationship of von Kármán (1946) for the torque coefficient of an unconfined, smooth rotating disk given as:

$$C_m = \frac{0.146}{Re_R^{1/5}} \tag{9}$$

The smooth disk C_m results show good agreement (within ±1%) with Eq. 9 over the entire range of Re_R. All of the rough disks exhibited significant increases in C_m. The epoxy-coated disk had an increase in C_m of 22–37% compared to the smooth disk values. The increases in C_m for the 220-grit and 60-grit sandpaper surfaces were 88–116% and 150–179%, respectively. The reason for the larger increases observed in C_m compared to C_f on the

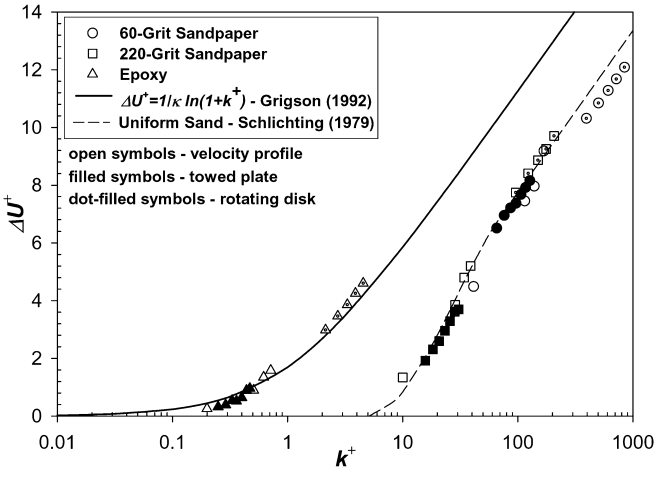

Fig. 8. Roughness function for the test surfaces obtained using the three methods. (Overall uncertainty in ΔU^+: velocity profile method, ±10% or 0.2 (whichever is greater); rotating disk method, ±9% or 0.3 (whichever is greater); towed plate method, ±12% or 0.2 (whichever is greater))

same surface was that the rotating disk experiments were conducted at unit Reynolds numbers of up to five times higher than the velocity profile experiments. This leads to an increased effect for a roughness of a given height.

Figure 7 shows the results of the towed plate experiments. The Kármán–Schoenherr friction line (Schoenherr 1932) for the frictional resistance of a smooth flat plate is also presented. It is given as follows:

$$\frac{0.242}{\sqrt{C_F}} = \log\left(Re_L C_F\right) \tag{10}$$

The smooth plate C_F values agree within ±2% with the Kármán–Schoenherr friction line. The C_F values for the 220-grit and 60-grit sandpaper surfaces were increased significantly compared to the smooth plate values over the entire Re_x range. The increases in C_F for the 220-grit and 60-grit sandpaper surfaces were 17–30% and 66–83%, respectively. The C_F values for the epoxy-coated plate showed only modest increase compared to the smooth plate. At the highest Re_x, the increase was 6%, which is slightly greater than the combined uncertainty in the measurements.

The roughness functions for each of the test surfaces using the three determination methods are presented in Fig. 8. Shown for comparison is the Nikuradse-type roughness function for uniform sand given by Schlichting (1979). Also shown is the Colebrook-type roughness function for random roughness given by Grigson (1992) as follows:

$$\Delta U^+ = \frac{1}{\kappa}\ln\left(1 + k^+\right) \tag{11}$$

The chosen roughness length scale for the sandpaper surfaces was k=0.75R_t. This was the length scale suggested by Schultz and Flack (2003) for sandpaper roughness. The roughness length scale used for the epoxy surfaces was k=0.39R_a. This length scale was offered by Schultz and Flack (2003) as an appropriate one for a range of painted and sanded surfaces. It should be noted that the choice of k for a given roughness has no effect on the calculated ΔU^+ despite its apparent dependence on k through the $\Delta U^{+\prime}$ term in Eqs. 6 and 8. This is because the effect of changing k on ΔU^+ is to simply move the curve along the abscissa without changing its slope.

The roughness functions obtained using the velocity profile and towed plate methods show good agreement for all three rough surfaces. The epoxy surface follows a Colebrook-type roughness function using the roughness length scale used here. The sandpaper roughness results using these methods agree within their uncertainty with a Nikuradse-type roughness function. Since the rotating disk results were obtained at much higher unit Reynolds numbers than the other two methods, direct comparison of the results is not possible. However, using the rotating disk method, the epoxy surface again has ΔU^+ values that agree within their uncertainty with a Colebrook-type roughness function. The sandpaper surfaces have ΔU^+ values that agree within uncertainty with a Nikuradse-type roughness function. Furthermore, the experimental results for both sandpaper surfaces have slopes ($\Delta U^{+\prime}$) of ~1/κ, the slope the roughness function is expected to exhibit in the fully rough flow regime.

4 Conclusion

Three experimental methods have been used to determine the roughness function of several surfaces. The results for the velocity profile and towed plate methods show good agreement for all surfaces, with the epoxy surface following a Colebrook-type roughness function and the sandpaper surfaces following a Nikuradse-type roughness function. Although the tests using the rotating disk method were carried out at much higher unit Reynolds numbers, the results for the sandpaper rough surfaces agree within their uncertainty with a Nikuradse-type roughness function in the fully rough regime, while the results for the epoxy surface agree with a Colebrook-type roughness function. The present results illustrate the utility of indirect methods in roughness function determination and also indicate that the rotating disk method may provide a relatively economical means for determining the effect of surface roughness at high Reynolds number.

References

Acharya M, Bornstein J, Escudier MP (1986) Turbulent boundary layers on rough surfaces. Exp Fluids 4:33–47

Antonia RA, Krogstad P-Å (2001) Turbulence structure in boundary layers over different types of surface roughness. Fluid Dynam Res 28:139–157

Clauser FH (1954) Turbulent boundary layers in adverse pressure gradients. J Aeronaut Sci 21:91–108

Colebrook CF (1939) Turbulent flow in pipes with particular reference to the transition between smooth and rough pipe laws. J Civil Eng 11:133–157

Coleman HW, Steele WG (1995) Engineering application of experimental uncertainty analysis. AIAA J 33:1888–1896

Coles D (1962) The turbulent boundary layer in a compressible fluid. Report R-403-PR, The Rand Corp.

Granville PS (1958) The frictional resistance and turbulent boundary layer of rough surfaces. J Ship Res 1:52–74

Granville PS (1982) Drag-characterization method for arbitrarily rough surfaces by means of rotating disks. J Fluids Eng 104:373–377
Granville PS (1987) Three indirect methods for the drag characterization of arbitrarily rough surfaces on flat plates. J Ship Res 31:70–77
Grigson CWB (1992) Drag losses of new ships caused by hull finish. J Ship Res 36:182–196
Hama FR (1954) Boundary-layer characteristics for rough and smooth surfaces. Trans SNAME 62:333–351
Klebanoff PS, Diehl FW (1951) Some features of artifically thickened fully developed turbulent boundary layers with zero pressure gradient. NACA TN 2475
Ligrani PM, Moffat RJ (1986) Structure of transitionally rough and fully rough turbulent boundary layers. J Fluid Mech 162:69–98
Loeb GI, Laster D, Gracik T (1984) The influence of microbial fouling films on hydrodynamic drag. In: Costlow JD, Tipper R (eds) Marine biodeterioration, an interdisciplinary study. Naval Institute Press, Annapolis, Md., pp 88–94
Moffat R J (1988) Describing the uncertainties in experimental results. Exp Thermal Fluid Sci 1:3–17
Nikuradse J (1933) Laws of flow in rough pipes. NACA TM 1292
Perry AE, Li JD (1990) Experimental support for the attached-eddy hypothesis in zero-pressure gradient turbulent boundary layers. J Fluid Mech 218:405–438
Raupach MR, Antonia RA, Rajagopalan S (1991) Rough-wall turbulent boundary layers. Appl Mech Rev 44:1–25
Schlichting H (1979) Boundary-layer theory, 7th edn. McGraw-Hill, New York
Schoenherr KE (1932) Resistances of flat surfaces moving through a fluid. Trans SNAME 40:279–313
Schultz MP (2002) The relationship between frictional resistance and roughness for surfaces smoothed by sanding. J Fluids Eng 124:492–499
Schultz MP, Flack KA (2003) Turbulent boundary layers over surfaces smoothed by sanding. J Fluids Eng 125: in press
von Kármán T (1946) On laminar and turbulent friction. NACA TM 1092